LA-UR- 08-4628

Approved for public release; distribution is unlimited.

Title:	Seismic Tomography of Pg and Sg/Lg and its use for Average Upper Crustal Structure in Eurasia
Author(s):	Lee K. Steck, W.S. Phillips, K. Mackey, M.L. Begnaud, R.J. Stead, C.A. Rowe
Intended for:	Publication in the Bulletin of the Seismological Society of America

Los Alamos
NATIONAL LABORATORY
EST. 1943

Form 836 (7/06)

Seismic Tomography of Pg and Sg/Lg and its use for Average Upper Crustal Structure in Eurasia

L. K. Steck, W. S. Phillips, K. Mackey[1], M. L. Begnaud, R. J. Stead, and C. A. Rowe

Los Alamos National Laboratory
Michigan State University[1]

For submission to Bulletin of the Seismological Society of America or Geophysical Journal International

Abstract

Tomographic inversion of travel times from first arriving compressional and shear waves for velocity structure has been applied with great success at all length scales, ranging from the laboratory bench-top to the entire Earth. Inversion of later arriving phases has seen a much more limited application. In this paper we present inversion results for regional Pg and Sg for the Eurasian continent to explore its use for understanding average upper crustal velocity structure. Inversion is performed using a damped, smoothed LSQR implementation that solves for site and event terms as well as for velocity along great circle paths between the source and receiver. Results are broadly consistent with published upper crustal velocities for the region. A spot-comparison of Vp/Vs from local and regional studies also compares well with the ratio of observed Pg to Sg velocities from our study where resolution is high. Resolution is determined through the use of checkerboard tests, and these suggest that in regions where data density is high we can resolve features down to at least 2 deg, with 4 deg possible over broader areas. RMS residual reductions are on the order of 25% for Sg and 30% for Pg.

Introduction

Inverting first arriving Pg travel times for crustal structure is widely used, both in refraction experiments and in smaller scale seismic deployments of one or two degrees aperture. Less common is the use of Sg/Lg and Pg for tomography at regional or continental scales. The primary reason for this is a lack of absolute certainty in the paths that these phases traverse. And, while first P is an obvious phase to identify, it is likely that different analysts in different regions will pick the largest secondary arrival as Pg, perhaps without knowing for certain the nature of the phase being thus labeled. Sg/Lg is easier to identify than Pg and appears more consistently picked. Despite these limitations, there are substantial observations of Pg and Sg/Lg available, representing a potential wealth of information on crustal structure. With the difficulties of such an experiment in mind, our intention is to explore the nature of these observations through tomography with the goal of identifying average upper crustal compressional and shear velocity structure in our study area.

The International Association of Seismology and Physics of the Earth's Interior (IASPEI) definition of Pg is as follows: "At short distances, either an upgoing P wave from a source in the upper crust or a P wave bottoming in the upper crust. At larger distances also arrivals caused by multiple P-wave reverberations inside the whole crust with a group velocity around 5.8 km/s."

(Storchak et al., 2003). In the IASP91 Pg tables (Kennett and Engdahl, 1991), travel times are defined only for events within the crust, which has a thickness of 35 km. In IASP91, Pg velocities for events in the crust are asymptotic to 6.1 km/s at distances of 1000 km. From 250 to 1000 km, Pg velocity ranges between 6.0 to 6.1 km/s. At distances between 100 and 250 km, Pg velocity ranges from 5.8 to 6.1 km/s. Travel time variations arising from event depth within the crust are less than about 1.5 s beyond distances of 75 km. Sg is defined by IASPEI as "At short distances, either an upgoing S wave from a source in the upper crust or an S wave bottoming in the upper crust. At larger distances also arrivals cause by superposition of multiple S-wave reverberations and SV to P and/or P to SV conversions inside the whole crust". Lg is the later arriving superpositional wave train, with a maximum energy group velocity of around 3.5 km/s. In IASP91, the Sg travel time tables have a phase velocity of very nearly 3.8 km/s, out to the maximum range of 957 km. In contrast, IASP91 Lg has a phase velocity of 3.5 km/s. Because Lg is contained in the Sg definition, from here on out we will largely refer only to Sg in our analyses. Lg will be called out only when we need to draw its distinction from the more general term, Sg.

Data and Method

Data for this study come from the Ground-based Nuclear Explosion Monitoring Research Knowledge Base at Los Alamos National Laboratory (LANL). This database consists of integrated local, regional, and global catalogs with arrivals sorted and merged by event. The largest bulk of the data come from the global catalogs of the United States Geological Survey Earthquake Data Reports (http://earthquake.usgs.gov/regional/neic), the International Seismic Centre (http://www.isc.ac.uk), and the Incorporated Research Institutions for Seismology Data Management Center (http://www.iris.edu). Other large regional catalogs include the preliminary Annual Bulletin of Chinese Earthquakes from the Chinese Seismological Bureau and several published and unpublished catalogs from northeast Russia. The epicentral ground truth (GT) of each event is tested using the Bondar et al., 2004 criteria and we identify about 10-20% of our events as having epicenters that are GT25 or better, that is, known to within at least 25 km of the true epicenter. GT events tend to be the largest events with highest signal-to-noise ratios and the clearest phase identifications. Time-distance plots of our GT datasets are shown in Figure 1, along with the IASP91 Pg and Lg travel time predictions, indicated by the heavy dashed lines. The time-distance plots reveal contamination from misidentified P and S arrivals, multiples of 60 s reporting errors, and bad arrival time picks. These data are eliminated using upper and lower bounds on acceptable slownesses. Some contamination is inevitable near the Pg/Pn and Sg/Sn crossovers. Figure 2 shows stations, events, and raypaths for the two datasets. For Pg, we have 3709 stations, 407131 events, and 1,453318 travel times. For Sg, there are 3084 stations, 266751 events, and 1,049125 travel times.

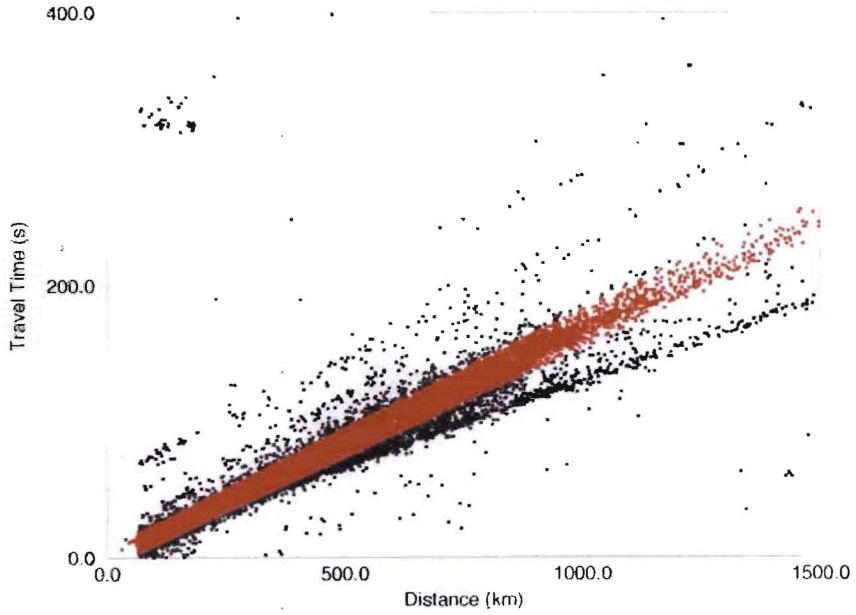
400.0
200.0
0.0
Travel Time (s)
0.0
500.0
1000.0
1500.0
Distance (km)

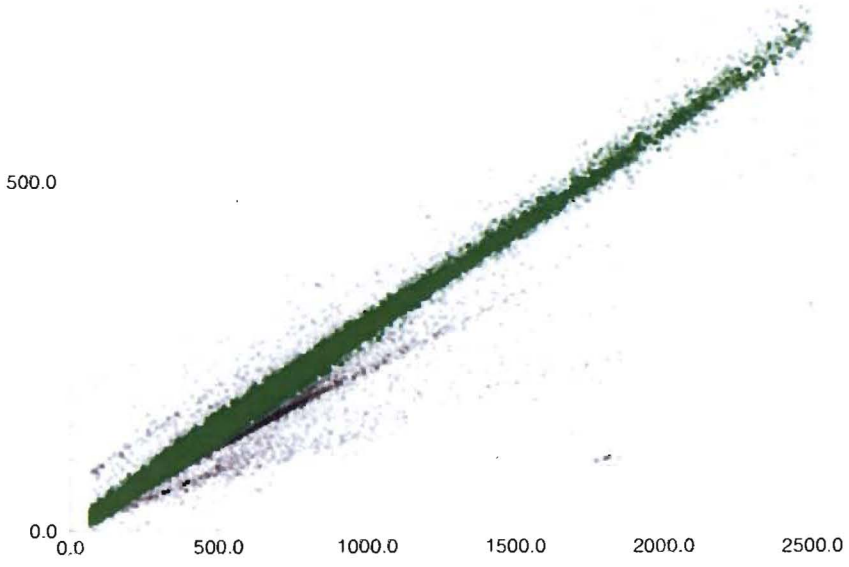
500.0
0.0
0.0
500.0
1000.0
1500.0
2000.0
2500.0

Figure 1. For GT25 or better data: a) time distance plot of the raw Pg data (black) and the data selected for our study (red). Contamination from misidentified Pn, Sn, and 60 s errors are evident. b) Similar plot for Sg, with selected data in green. Misidentified phases here include Sn and Pg.

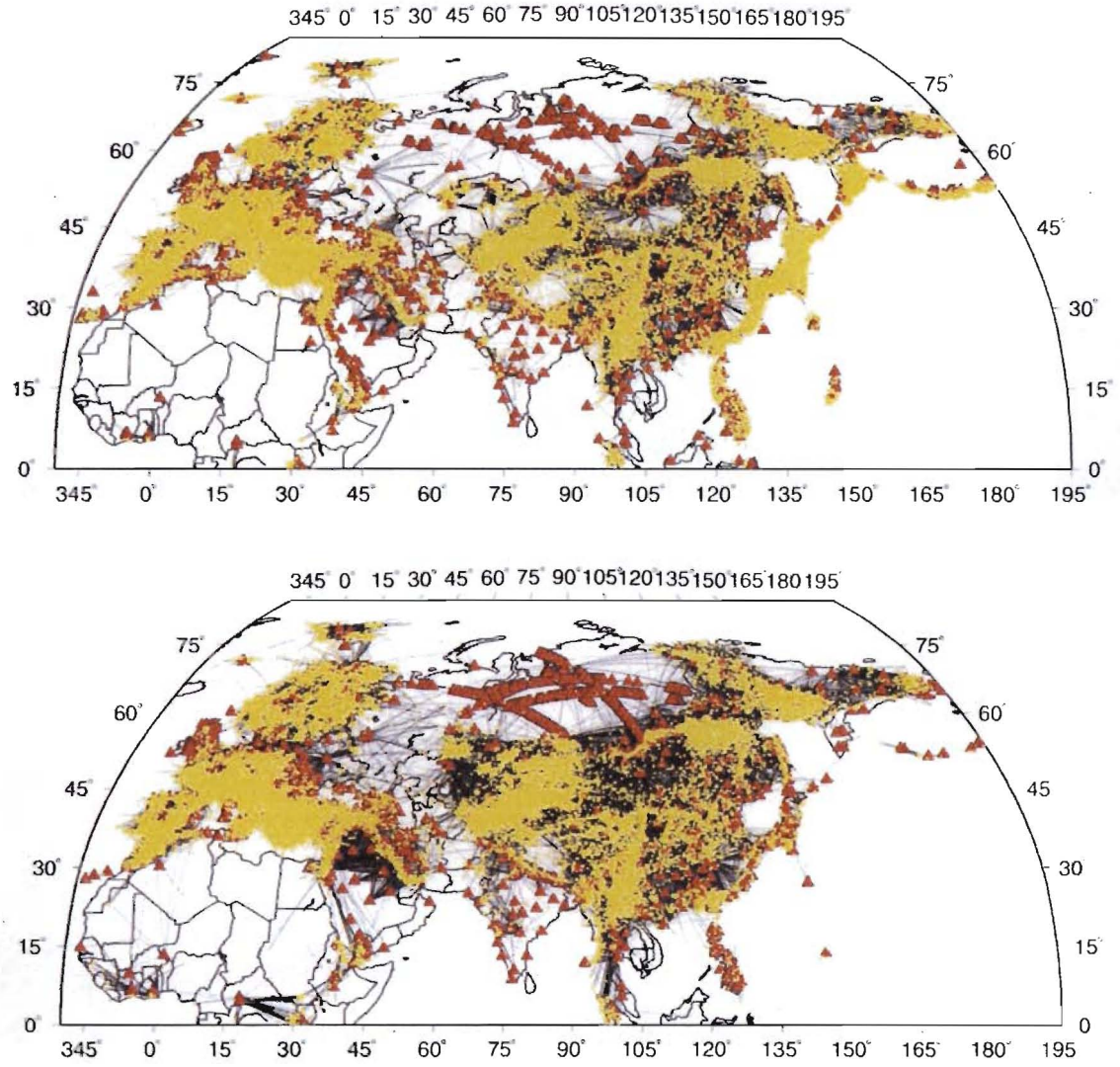

Figure 2. Stations (red triangles), events (yellow dots), and ray paths (black lines) for all data used: top is Pg and bottom is Lg.

To invert this dataset, we use a method analogous to Pn tomography, whereby we assume a great circle path between source and receiver. Events are restricted to depths less than 33 km and stations are constrained to be at distances between 0.6 and 14 deg from the epicenter for Pg and 0.6 and 24 deg for Sg. To accommodate depth uncertainty and near-receiver velocity effects we solve for both an event term, e, and a site term, r, and we damp the site term sum to zero. Travel times for the i^{th} event to the j^{th} station are expressed as:

$$t_{ij} = \Sigma\, \delta x_l s_l + e_i + r_j,$$

where the δx_l are path segments and the s_l are slownesses for those segments. The summation is taken over the n segments of the great circle path. Observed travel times are weighted by the square root of the GT level, with a minimum GT level set to 1km. Events which did not have a Bondar et al., 2004 GT level were assigned a value of 50 km. In our solution, we employ first difference regularization over a 1 by 1 deg grid, and solve the set of equations using the LSQR conjugate gradient method (Paige and Saunders, 1982). We invert for slowness over a region spanned by latitudes from 0 to 80 deg N and longitudes from -20 to 195 deg E.

Resolution Tests

To provide insight into the resolving power of our datasets, we look at our ability to recover checkerboard velocity anomalies using the available ray paths. Tests were run for checkerboards with 2, 4, and 10 deg squares with velocities alternating between +/- 10% perturbations. Coverage with good resolution is better for Sg than for Pg largely due to the longer ray paths of Sg phases. Figure 3 shows results from inversion of the synthetic checkerboard times for the 2, 4, and 10 deg patterns for both Pg and Sg. For Sg, good resolution is obtained for the bulk of China and Mongolia, extending up into Northeastern Russia, and westward into Kazakhstan. Europe and Scandinavia are also well covered. Some limited resolution is found in the Middle East and Western India. Compared to Sg, Pg resolution is reduced in all regions. At 2 deg, only the regions with the densest ray path coverage are resolved. This includes parts of western Europe, from Spain up to southern Germany and down through Greece and south-central China.

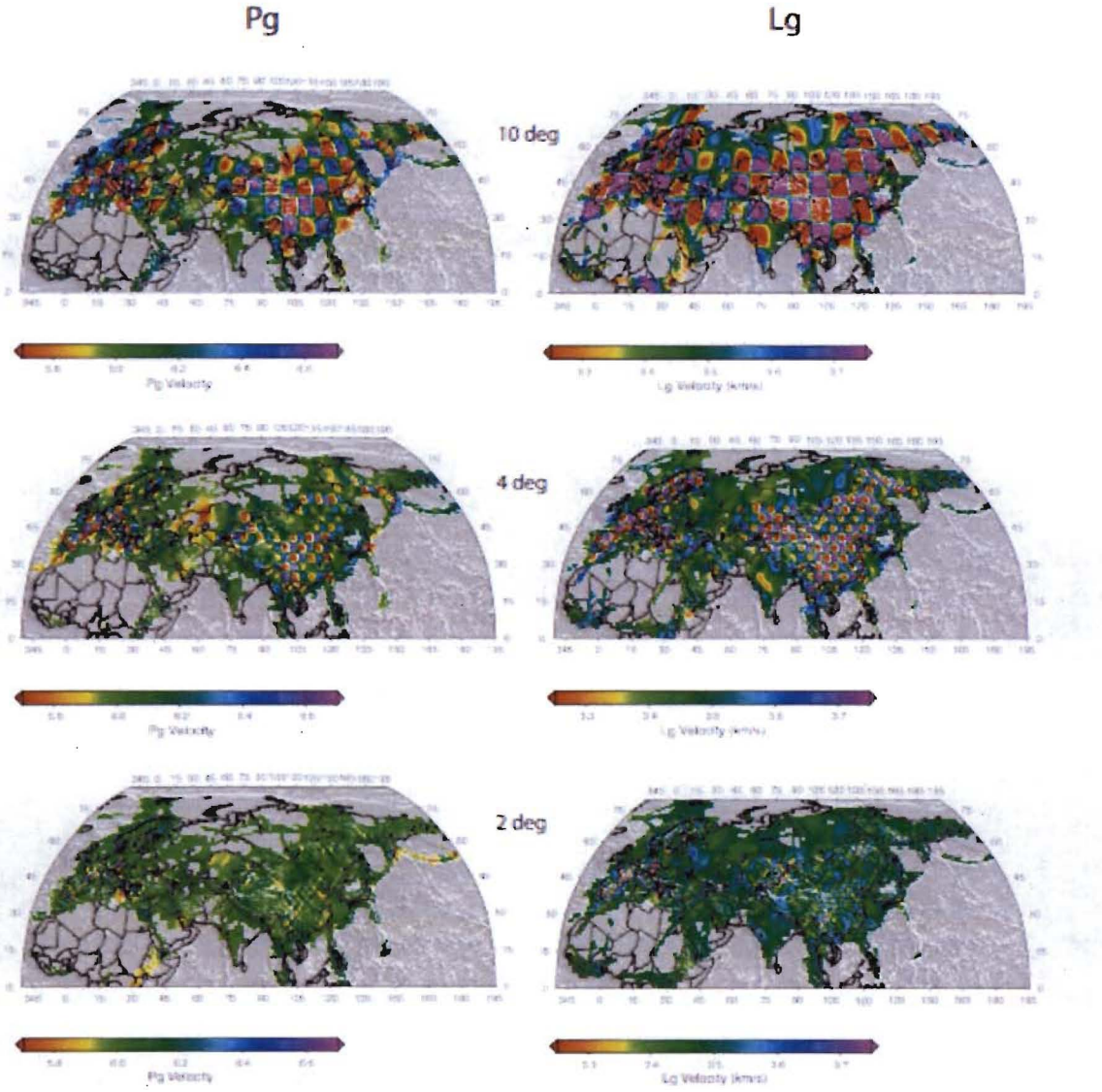

Figure 3. Two, four and ten degree checkerboard resolution tests for Pg (left column) and Sg (right column).

Results

Inversion results for Pg and Sg are shown in Figure 4. Obvious trends in Pg velocity can be observed: 1) regions with convergent tectonics, i.e. the Pacific Rim, exhibit faster than average apparent Pg velocity. 2) The bulk of Asia, from 75 deg E longitude to the continental margin exhibits average to slightly fast apparent Pg velocities. 3) Slow velocities are found in the Middle East, including India, Pakistan, Iran, Iraq, and north to Kyrgyzstan, the Caspian Sea region, and the lower Volga. Scandinavia is average to fast, while the rest of Europe, with the exception of Sicily, Spain and perhaps central Turkey is slow. For Sg, the bulk of Eurasia is faster than average, with lower velocities in the Tibetan Plateau, the Gulf of Oman and parts of the Middle East, parts of eastern Europe, central and north-central Russia, and Sakhalin Island.
We compute Vp/Vs ratios by taking the ratio of the Pg and Sg velocity maps. This is shown in Figure 5. High Vp/Vs ratios are found in Tibet, parts of south-east China, and in the island arcs of the western Pacific. Low Vp/Vs is observed in parts of eastern Europe, and in the eastern Mediterranean and the Afar Triangle. Resolution for Pg is very low in India, so Vp/Vs ratios there should be ignored.

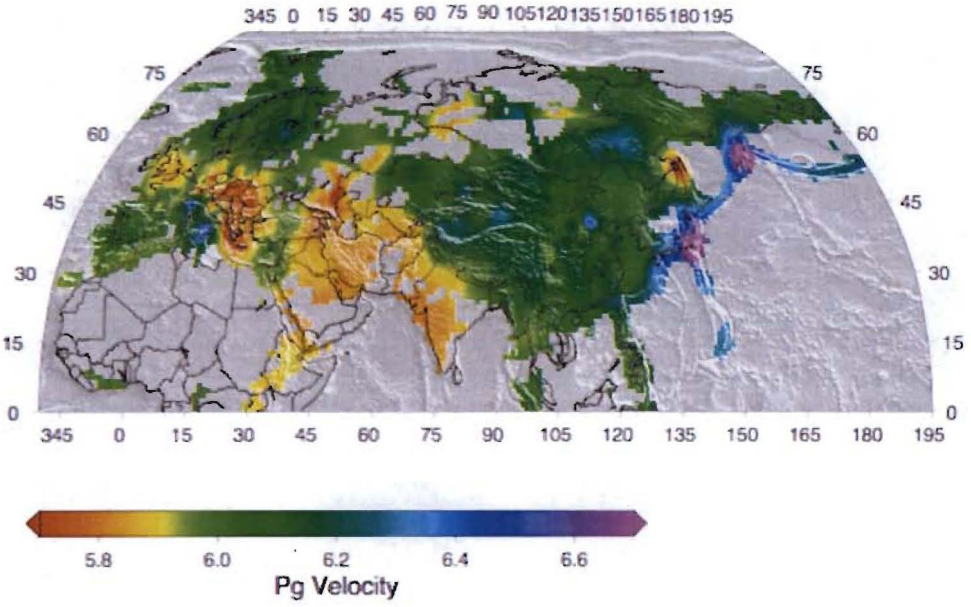

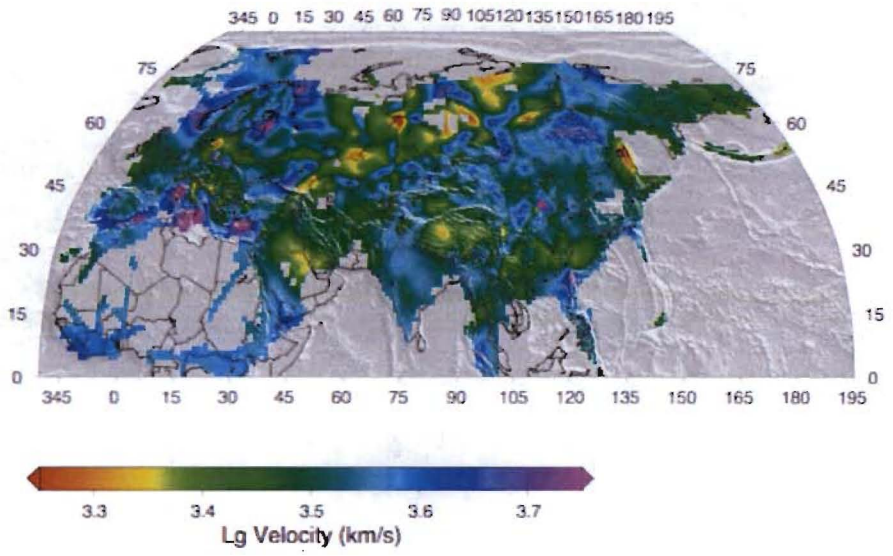

Figure 4. Top: Pg travel time inversion results for Eurasia. Bottom: Sg travel time inversion results for Eurasia. Results at grid points with hit counts less than 2 are not plotted.

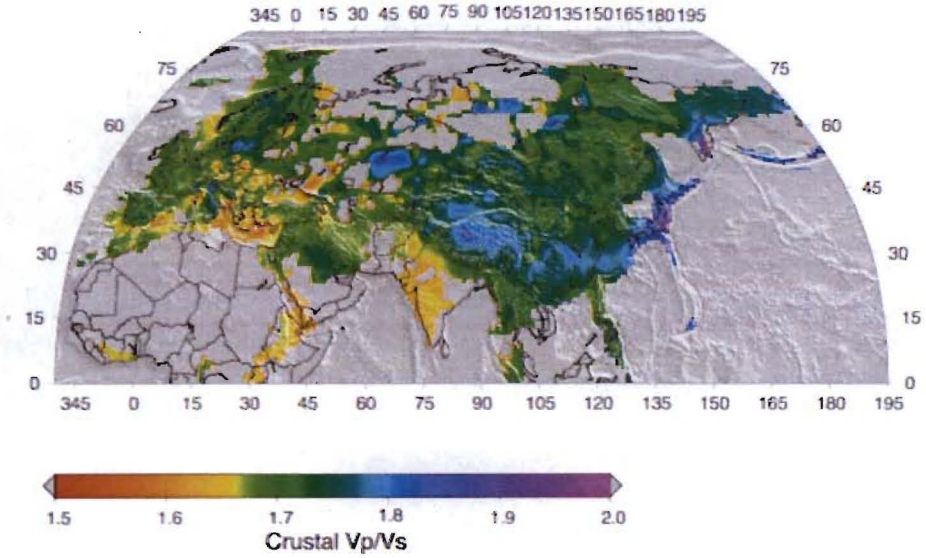

Figure 5. Vp/Vs ratio for Eurasia.

Station terms (Figure 6) are damped to 0.0 and have a standard deviation of 1.28 s for Pg and 2.62 s for Sg. We show a block median smoothed representation of these terms to demonstrate regional trends and consistency between Pg and Sg results. Minimum/maximum terms are -15/9.2 s for Pg and -24/ 31 s for Sg. Despite some outliers, broad trends are seen in these terms. Station terms are negative in the bulk of China, parts of Russia and Siberia, and Iraq. High station terms are found in Western Europe, Nepal, and in the western Pacific Rim. Particularly high values are found in Poland. We interpret the station terms to reflect variations in the sedimentary layer above the upper crust, with fast stations representing thinner sediments and slow stations thicker sediments. Figure 7 shows sediment thickness from the Crust2.0 model of Bassin et al. (2000).

The average event terms are less than 0.009 s for both Pg and Lg, with standard deviations of .3 and .65 s respectively for Pg and Sg. Block median smoothed event terms are shown in Figure 8. Unsmoothed minimum/maximums for Pg and Sg are -13.2/7.8 and -18.7/22.1 respectively. The greatest variability is seen in northern Russia where coverage is poor.

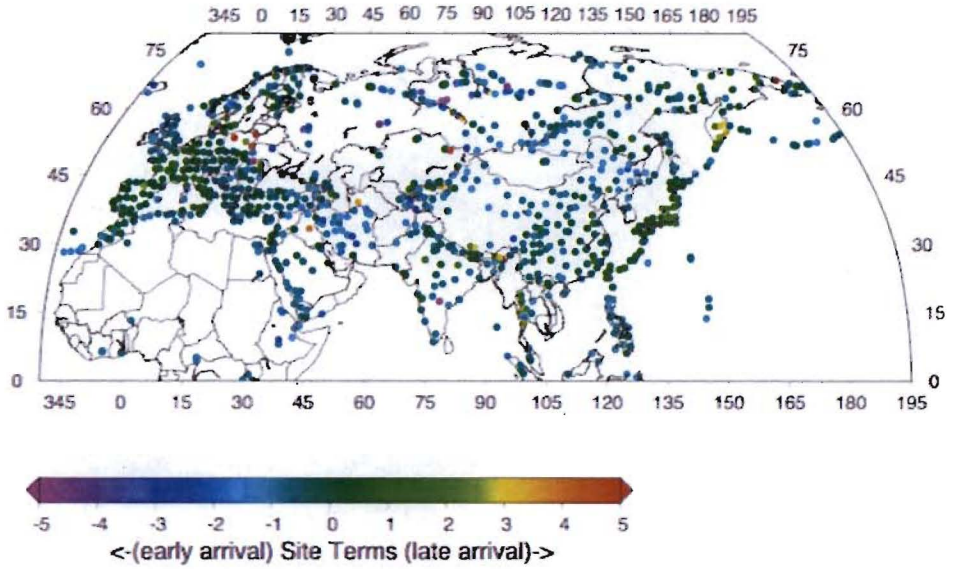

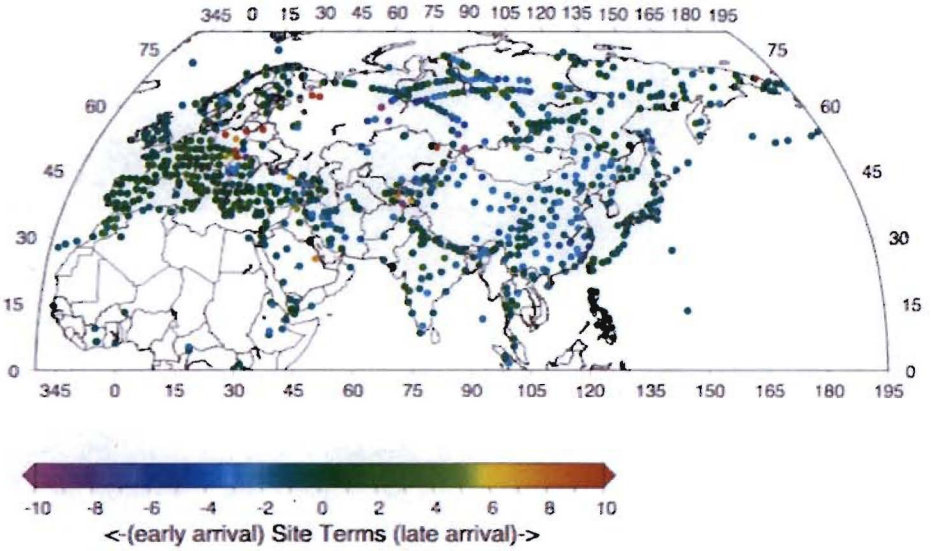

Figure 6. Station terms smoothed using a 2 deg block median filter to show geographic trends. Top: Pg, bottom: Sg. Note similarity in patterns, with Sg having about double the station term sizes compared to Pg.

Figure 6. Station terms smoothed using a 2 deg block median filter to show geographic trends. Top: Pg, bottom: Sg. Note similarity in patterns, with Sg having about double the station term sizes compared to Pg.

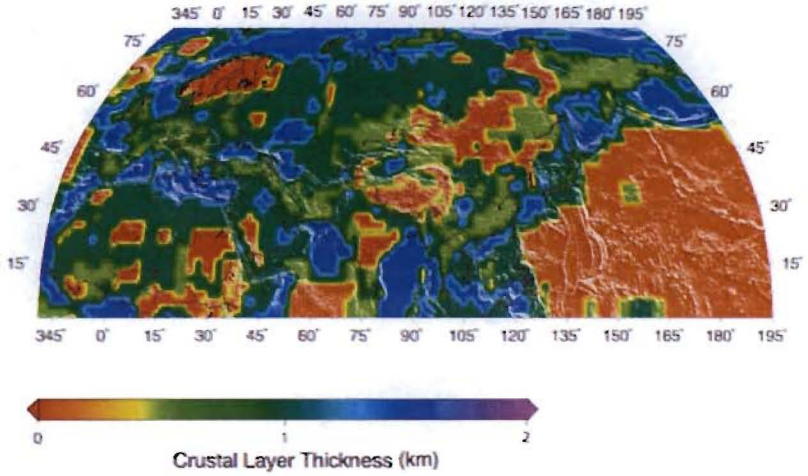

Figure 7. Sediment depths from CRUST2.0.

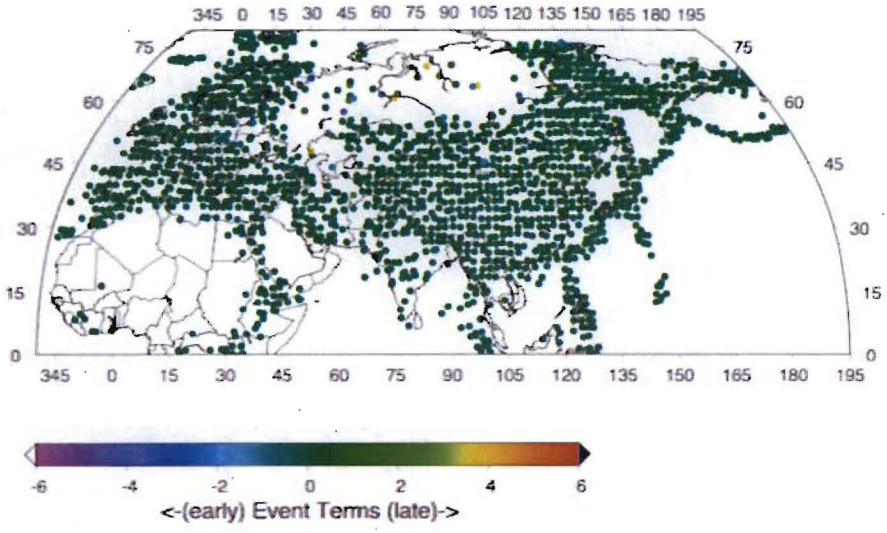

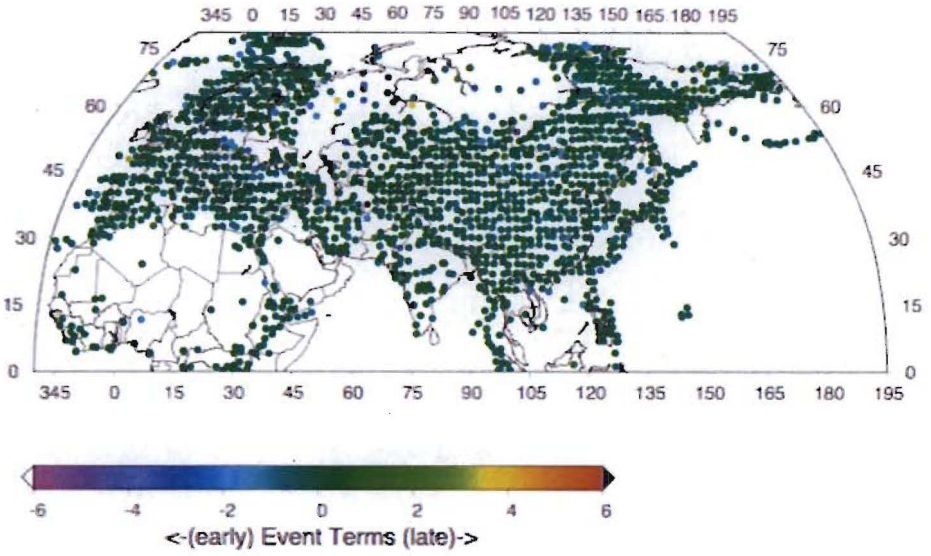

Figure 8. Event terms, smoothed with 2 deg block median filter to show geographic trends. Top: Pg, bottom: Sg.

Discussion

Our Pg results are broadly consistent with many observations. Average velocities and large scale heterogeneity are largely consistent two apriori upper crustal models: Crust2.0 and the Department of Energy (DOE) Unified Model, a merger of Lawrence Livermore National Laboratory's Western Europe North Africa model (Pasyanos et al., 2004) and the China East Asia model from Los Alamos National Laboratory (Begnaud et al., 2005). For example, we observe an increase in velocity moving north and east across the Trans European Suture Zone into Fennoscandia and the Ukranian Shield, from an average Pg velocity of 5.8 km/s to 6.0 km/s and greater. A similar jump is seen in upper crustal velocities in Crust2.0 and the Unified Model, though from 6.1 to 6.2 km/s (Figure 9 shows the DOE Unified Model for the upper crust). Both models also show lower velocities in Turkey and Iran. We see a similar pattern, and our results in Iran do match those of receiver functions from the Zagros Mountains reported by Hatzfeld et al. (2003). However, our resolution in that region is poor. Li and Mooney (1998) give average crustal velocities for China of 6.1 – 6.45 km/s, while ours range from 6.0 – 6.3 km/s. Recent results from the Mediterranean west of Italy show high velocities off the toe of Italy with lower velocities emerging northwest towards Sardinia (Margheriti et al., 2008), as we observe. Discussions with Russian seismologists from Sakhalin Island confirm that both P and S wave velocities there are low (K. Mackey, Pers. Comm.). We see overall agreement with Piromallo and Morelli (2003) for Europe, though our model is smoother, and we don't see pronounced high velocities in eastern Europe. Theirs is a combined regional and teleseismic first P result that has nodes at 0 km, 50 km, and so on down to 1000km. Some smearing of the mantle up into the topmost node has likely occurred. In the British Isles, higher mid to upper crustal velocities are

observed in the north than in the south in wide angle seismic studies (Champion et al., 2006) with an average upper crustal velocity in the south of about 5.8-5.9 km/s, similar to what we observe in this study. In general, our resolution is low in India, southern Pakistan and Afghanistan, northern Russia, and Iraq, except perhaps at the tip of the Gulf of Oman.

For Sg, we see a small jump in velocities across the TESZ, though it isn't as prominent as the Pg transition we observe there. This again agrees with the trend seen in the Unified Model. Lower Sg velocities continue down from eastern Europe through Turkey and Iran and into the Tibetan Plateau and south eastern China. We also find lower velocities in eastern Mongolia that extend into northern China. A similar feature is seen in the Unified Model but containing significantly lower velocities.

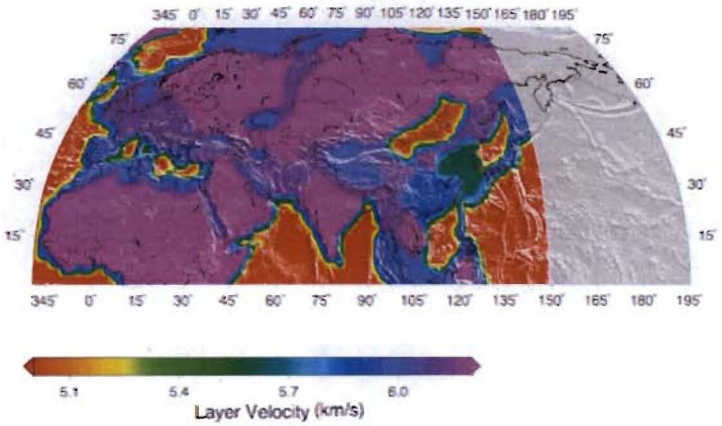

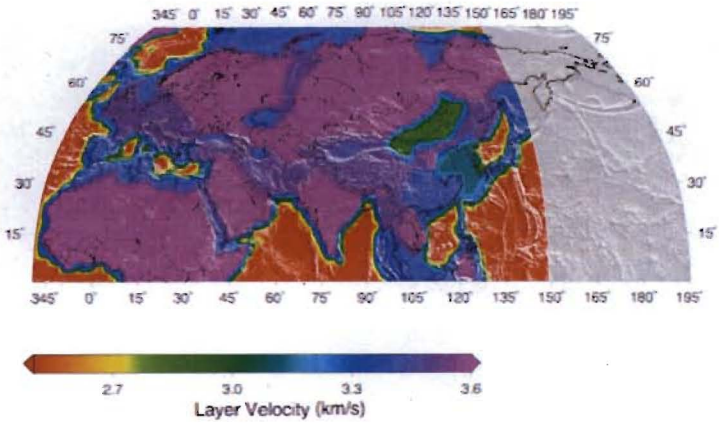

Figure 9. Top: P velocities for the DOE Unified Model upper crust. Bottom: S velocities in upper crust of the DOE Unified Model.

Spot checks of our Vp/Vs map correspond well with results from local and regional studies of upper crustal Vp/Vs, largely from tomography and receiver function studies, and this is summarized in Table 1.

Table 1. Comparison of published Vp/Vs ratios and ratios from this study

Location	Published Values	This Study
Chugoku, Japan (Ramesh et al., 2005)	1.85-2	1.9
Tibet (Zhu et al., 1998)	1.8-2.0	1.8
Dead Sea Transform (Koulakov&Sobolev, 2006)	1.72	1.7
Aegean Sea (Zhu et al., 2006)	1.73	1.73
Turkey (Zhu et al., 2006)	1.82	1.78
Arabian Platform (Al-Damegh et al., 2004)	1.8	1.77
Iberian Massif (Jordi, 2007)	1.72	1.7
Northwest Poland (Grad et al., 2006)	1.7	1.75
Alps (Kummerow et al., 2004)	1.73	1.75

Overall, there is good agreement between major trends in our observed Pg and Sg velocity maps, and published results for upper crustal velocities for locations around Eurasia, though our study extends these results to new regions (e.g. Siberia) and provides a single comprehensive velocity map. For Pg, our average travel time is larger than Pg travel times predicted by AK135 at distances beyond 500km. For Sg, our average travel time is well modeled by the AK135 Lg travel time curve, out to 2500 km. Simple one and two bounce P and S crustal multiples (e.g. PmP and PmPPmP) in AK135 and in thicker models for China such as LMV (Steck et al., 2001) and SSB (Jih, 1998), do not fit our observations well, predicting later times within 500 km distance and earlier times beyond that distance. The fit is worse for Sg than Pg. With a superposition of limited travel time segments from four or more Moho reverberations it is likely possible to fit our results with almost any crustal model or combination of crustal models at distances past 500 km. This inherent non-uniqueness makes inverting Pg or Sg in terms of crustal multiples relatively intractable. Our results suggest that Pg and Sg can be coherently inverted using a simple model of upper crustal velocity structure. Our goal is to use these models to calibrate Pg and Sg travel times for seismic event location in Eurasia.

Data and Resources

Most data for this study come from the United States Geological Survey Earthquake Data Reports, the International Seismic Center, and the Incorporated Research Institutions for Seismology Data Management Center. However, some data are not releasable.

Acknowledgments

We thank Paul Wessel for use of the GMT graphics software package. This research supported by the US DOE under contract W-7405-ENG-36, LA-UR-08-XXXX.

References

Al-Damegh, Khaled, E. Sandvol, A. Al-Lazki, and M Barazangi (2004), Regional seismic wave propagation (Lg and Sn) and Pn attenuation in the Arabian Plate and surrounding regions, *Geophys. J. Int.*, 157, 775-795.

Bassin, C., G. Laske, and G. Masters (2000), The current limits of resolution for surface wave tomography in North America, *EOS Trans. AGU*, 81, F897.

Begnaud, M.L., C.A. Rowe, L.K. Steck (2004) Validating three-dimensional models in China and East-Asia for use in regional seismic event location, *Eos Trans. AGU*, 85(47), Fall Meet. Suppl., T11C-1277.

Bondar, I, S. C. Myers, E. R. Engdahl, and E. A. Bergman (2004), Epicenter accuracy based on seismic network constraints, *Geophys. J. Int.*, 156, 483-496.

Champion, M.E. Shaw, N.J. White, S.M. Jones and K.F. Priestley, (2006) Crustal velocity structure of the British Isles; a comparison of receiver functions and wide-angle seismic data, *Geophys. J. Int.*, 166, 2, 795-208.

Grad, M, T. Janik, A. Guterch, P. Sroda, W. Czuba and the EUROBRIDGE'94-97, POLONAISE'97, and CELEBRATION 2000 Seismic Working Groups (2006), Lithospheric structure of the western part of the East European Craton investigated by deep seismic profiles, *Geol. Quarterly*, 50, 9-22.

Hatzfeld, D, M. Tatar, K. Priestley, M. Ghafory-Ashtiany (2003), Seismological constraints on the crustal structure beneath the Zagros Mountain belt (Iran), *Geophys. J. Int.*, 155, 403-410

Jih, R.S., (1998), Location calibration efforts in China, *Proceedings for the 20th Annual Seismic Research Symposium*, pp12.

Jordi, J (2007), Constraining velocity and density contrasts across the crust-mantle boundary with receiver function amplitudes *Geophysical Journal International* 171 (1) , 286–301 doi:10.1111/j.1365-2966.2007.03502.x

Kennett, B. L. N. and E. R. Engdahl (1991), Traveltimes for global earthquake location and phase identification, *Geophys. J. Int.*, 105, 429-465.

Koulakov, I, and S. V. Sobolev (2006) Moho depth and three-dimensional *P* and *S* structure of the crust and uppermost mantle in the Eastern Mediterranean and Middle East derived from tomographic inversion of local ISC data *Geophys. J. Int.* 164 (1), 218–235 doi:10.1111/j.1365-246X.2005.02791.x

Kummerow, J, R. Kind, O. Oncken, P. Giese, T. Ryberg, K. Wylegalla, F. Scherbaum, and TRANSALP Working Group (2004), A natural and controlled ource seismic profile through the Eastern Alps: TRANSALP, *Earth and Planet. Sci. Letts.*, 225, 115-129.

Li, S. and W.D. Mooney (1998), Crustal structure of China from deep seismic sounding profiles *Tectonophysics*, 288, 105-113.

Margheriti, L, and members of the Messina 1908-2008 team, (2008), Understanding crust dynamics and subduction in southern Italy, *EOS Trans AGU*, 89, 225-226.

Paige, C. C., and M. A. Saunders (1982), Algorithm 5583, LSGR: Sparse linear equations and least-squares problems, *Trans. Math. Software*, 8, 195-209.

Piromallo, C., and A. Morelli, (2003) *P* wave tomography of the mantle under the Alpine-Mediterranean area, *J. Geophys. Res.*, *108*(B2), 2065, doi:10.1029/2002JB001757

Pasyanos, M.E., W.R. Walter, and M.P. Flanagan (2003), Geophysical models for nuclear explosion monitoring, *Proceedings of the 25th Seismic Research Review*, Tuscon, AZ, 125-134.

Ramesh, D. S., H. Kawakatsu, S. Watada, and X. Yuan (2005), Receiver function images of the central Chugoku regiona in the Japanese islands using Hi-net data, *Earth Planets Space*, 57 271-280.

Steck, L.K., A. A. Velasco, A. H. Cogbill, and H. J. Patton, 2001. Improving regional seismic event location in China, *Pageoph.*, 158, 211-240.

Storchak, D. A. and members of the IASPEI Working Group on Phase Names (2003), IASPEI standard seismic phase list, *Seism. Res. Lett.*, 74, 769-770.

Zhu, L, (1998), Broadband waveform modeling and its application to the lithospheric structure of the Tibetan Plateau, *Phd Dissertation*, California Institute of Technology.

Zhu, L, B.J. Mitchell, N. Akyol, I Cemen, K. Kekovali (2006), Crustal thickness variations in the Aegean region and implications for the extension of continental crust, *J. Geophys. Res.*, 111, B01301, doi:10.1029/2005JB003770